Journal of The Electrochemical Society, **160** (6) B83-B89 (2013)
0013-4651/2013/160(6)/B83/7/$31.00 © The Electrochemical Society

Methane Recognition and Quantification by Differential Capacitance at the Hydrophobic Ionic Liquid-Electrified Metal Electrode Interface

Zhe Wang,[a,*] Xiaoyi Mu,[b] Min Guo,[a] Yue Huang,[b] Andrew J. Mason,[b] and Xiangqun Zeng[a,,z]**

[a]*Chemistry Department, Oakland University, Rochester, Michigan 48309, USA*
[b]*Department of Electrical & Computer Engineering, Michigan State University, East Lansing, Michigan 48824, USA*

We present a method to identify and quantify methane using a hydrophobic ionic liquid (IL)–electrified metal electrode interface by electrochemical impedance spectroscopy. We investigated the mechanisms of the responses of the IL-electrified electrode interface to the exposure of methane and other interfering gases (H_2, C_6H_{12}, SO_2, NO, NO_2, CO_2, O_2, H_2O). Our results show that at low frequency the IL-electrified electrode interface shows a predominantly capacitive response. The IL-electrode double layer (EDL) was found to be the primary response layer while the transition zone and bulk region of the IL-electrode interface contribute little to the overall signal change. For recognition and quantification of methane using the Langmuir adsorption model and measurement of differential capacitance change, an optimum EDL interface structure was found to form at a specific DC bias potential. The cumulative results shown in this work suggest that an ideal IL-electrode interface can be formed by varying IL structure and applied DC bias electrode potential for a specific analyte and that the semi-ordered structure of IL-electrified interface can act as a recognition element for the sensitive and selective adsorption and detection of gaseous molecules.
© 2013 The Electrochemical Society. [DOI: 10.1149/2.138306jes] All rights reserved.

Manuscript submitted January 4, 2013; revised manuscript received April 9, 2013. Published April 23, 2013.

Due to their unique properties and increasing availability, room temperature ionic liquids (ILs) have received great interests in electrochemistry, catalysis, electronics, and energy conversion as well as interdisciplinary investigations on both fundamental and practical applications.[1–5] For example, ILs as solvent free and ion-coupled material exhibit strong benefits as non-aqueous electrolytes for enhancing the safety and robustness for sensor and transistor devices.[6–12] However, the low intrinsic conductivity of the ILs correlates with their high viscosity, which limits the response time and sensitivity of detection methods such as those based on amperometry and potentiometry.[13–17] Methane, which has been considered as a clean energy source and one of the most important greenhouse gases, has attracted significant interest to the characterization of its adsorption on surfaces and its quantification in atmosphere as well. Since methane is relative chemically and electrochemically inert, current methods for methane detection are either relatively high-cost (e.g. optical), which prevents widespread deployment, or lack the selectivity (e.g. catalytic bead)[18] demanded by various applications. Many methane sensors also need improvement regarding their size, power consumption and the ease of use.[19–21]

Current results show that the potential-dependent interface of an IL and metal electrode is very sensitive to surface conditions on the electrode, such as the proton adsorption on an oxide electric interface[22] and the adsorption of CO on a metal electrode[23]. As shown in Figure 1, the molecular selectivity of an IL-electrode interface comes from the ordering of the electric double layer (EDL) as well as molecular interactions between the IL and analyte. Martin et al.'s Landau-Ginzburg-type continuum theory[24] for IL predicts overscreening at low DC bias and crowding of counter ions with an increase of the DC bias in a condensed inner layer near the electrode.[25–27] As reported in an IL-platinum interface,[23] the adsorption of gas molecules in the IL-electrified interface has been shown to lead to a change of the EDL capacitance that is attributed to a change of the EDL thickness.[28–30] We believe these phenomena based on IL's unique EDL have great implication for sensing and could rapidly quantify gas adsorption on the electrode, especially for inert gas. Besides the semi-ordered structure of IL EDL, the large, flexible, highly polarizable and chemically complex ions of IL could provide additional molecular selectivity via a number of inter-ionic forces including dispersion forces, dipole-dipole interaction, hydrogen bonding and pi-stacking forces in addition to Coulombic force. This wide range of molecular interactions allows for modification of the EDL via the rearrangement of adsorbed ions as the potential applied to the electrode changes.[25]

In contrast to the EDL typically observed in dilute electrolytes, IL ions are strongly oriented near the electrode into an ordered layer structure with local ion density at maximum possible value.[23] Multiple ion pair layers form at the interface.[27,31,32] Due to this heterogeneity, the lattice formation at the interface and the subsequent capacitance variations are not monotonic as described by the Gouy-Chapman-Sterns model. Additionally the hysteresis effects of an IL EDL, where the double layer capacitance depends on the scan direction of the DC potential, contributes to the slow pseudocapacitive process at the IL-electrode interface.[33] Therefore, the conditioning parameters for any practical applications based on the IL EDL need to be carefully studied. Adding more to this complexity, various physical and chemical factors can disrupt this highly ordered IL structure at the electrode interface. For instance, steric effects and adsorption of ions can occur at the IL-electrode interface, all influencing the structure and thickness of the EDL.[34,35] So far, no consistent equivalent circuit model has been developed to describe the impedance response of an IL-electrode interface for all possible conditions.

To validate IL EDL for gas sensing, we have addressed several critical issues of using IL EDL for characterizing selective gas adsorption. Firstly, to overcome small diffusion coefficients of gas molecules in ILs caused by the high viscosity of ILs[36], mesoporous gold electrodes were patterned on a planar gas permeable membrane, allowing gas analytes to reach the electrolyte-electrode interface directly without a diffusion pathway through the bulk IL. Additionally, the high surface area provided by mesoporous gold surface will lead to an increase of the double layer capacitance.[37] Secondly, in order to reduce the adsorption of ions in the IL at the IL-electrode interface, a unique IL, (1-butyl-1-methylpyrrolidinium bis(trifluoromethylsulfonyl)imide) ($[C_4mpy][NTf_2]$) was selected in this study. The bulkiness of tetrahedral quaternary ammonium cation forces the anions away from the cation. Furthermore, the delocalization of the negative charge along the –S-N-S- core of the NTf_2^- anion also reduces the cation and anion interaction. Compared with imidazolium-based IL, the specific functions of $[C_4mpy][NTf_2]$, such as sterical hindrance through alkyl groups, could be incorporated to minimize IL-electrode interactions and maximize compressibility of the solvation layers.[19–21] In addition, its hydrophobicity can minimize the possible interference and contamination from moisture.

We have systematically investigated methane adsorption/dissolution behaviors on the IL-electrode interface under a DC bias

*Electrochemical Society Student Member.
**Electrochemical Society Active Member.
zE-mail: zeng@oakland.edu

Downloaded on 2016-09-15 to IP 134.197.85.26 address. Redistribution subject to ECS terms of use (see ecsdl.org/site/terms_use) unless CC License in place (see abstract).

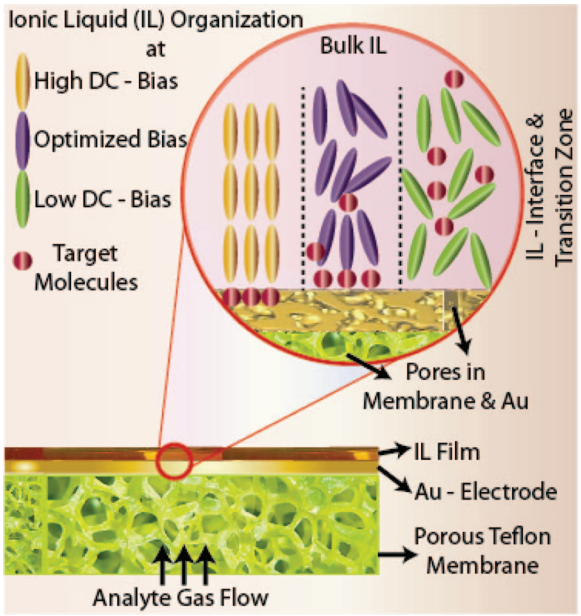


Figure 1. Schematic diagram of IL-electrified interface sensor response mechanism.

potential using electrochemical impedance spectroscopy (EIS). EIS provides a direct and non-invasive measurement of the redistribution of ions within the EDL under a fluctuating AC voltage with and without analyte present. At a low AC frequency and an optimized DC bias, the ordered static IL EDL on the electrode surface was identified for effective methane sensing. This is the first known report of the quantitative and selective detection of the target gas analyte based on an ordered IL EDL. The resulting understanding that the IL EDL structure can be tuned by the applied DC potential provides a great opportunity to develop a sensor array to detect multiple analytes with very few sensors. Additional parameters that can have strong impact on EDL structures can be used to further optimize sensor performance, such as changing the adsorption processes using different electrode materials that can affect the adsorption mechanisms. These studies are on-going in our laboratory.

Experimental

Reagents and materials.— POREX porous PTFE with 35% porosity and 4 μm pore size (Zitex TM, Chemplast, Incorporated, Wayne, New Jersey) was used as a gas permeable membrane. 300 nm-thickness of gold was thermal evaporated on PTFE with size of 0.75 inch × 0.5 inch by Edwards auto 306 evaporator (Edwards Ltd.), to precisely control the reaction, as well as to miniaturize the sensor. The porous Au electrodes provide particularly high surface areas (Figure S1). The working and counter electrodes were interdigited finger electrodes with a 200 μm gap. The quasi-reference electrode was fabricated in the same plane which enables the maintenance of a constant DC bias potential. The surface topography of electrode was measured by JEOL JSM-840 SEM (Figure S1). 1-butyl-1-methylpyrrolidinium bis(trifluoromethylsulfonyl) imide [C_4mpy][NTf_2] (Figure S2) was chosen as the electrolyte because it has low viscosity and high chemical stability, and it was prepared and refined to gravimetric purities exceeding 99.9% using reported methods[38–40]. A 200 μm thick layer of IL was coated on the electrodes by casting.

EIS experimental protocol.— The complex capacitance, $C(\omega) = C_{re}(\omega)\text{-}jC_{im}(\omega)$, where C_{re} and C_{im} are the real and imaginary capacitance values, can be calculated from the complex impedance $Z(\omega) = Z_{re}(\omega)\text{-}jZ_{im}(\omega)$ based on electrochemical impedance spectroscopy.[41] $C(\omega) = 1/j\omega Z(\omega)$, $C_{re} = -Z_{im}/(2\pi f (Z_{im}^2 + Z_{re}^2))$; $C_{im} = -Z_{re}/(2\pi f (Z_{im}^2 + Z_{re}^2))$. Here, f is the frequency, ω is the angular frequency. Abs C can be calculated as Abs $C = (C_{re}^2 + C_{im}^2)^{1/2}$. EIS experiments were carried out with a VersaStatMC (Princeton AMETEK, US) controlled by a Pentium-based PC running Windows XP and data were obtained using instrument attached software (VersaStudio). A DC bias potential of −0.3 V and an AC potential with 10 mV amplitude were applied at the working electrode. The total gas flow rates were maintained at 200 ± 0.05 sccm (standard cubic centimeters per minute) by digital mass-flow controllers (MKS Instruments Inc). The mass flow controllers were used to adjust the volume ratio of the testing gas flows, in which one is used to control the gas content by the volume per minute. Liquid samples were introduced into system as a vapor by allowing the carrying gas to flow through a gas-wash bottle filled with the liquid samples.

Quartz crystal microbalance (QCM).— The method of QCM characterization of the gas solubility in ILs was reported previously by our group.[42] Similar procedure was used here. Briefly, the aforementioned ILs were cast on both sides of the QCM (10 MHz, International Instruments, Oklahoma City, OK) from their ethanol solutions. Typical surface loading of ILs on QCM surfaces were in the ∼5 μg range that yields an IL film of tens to ∼200 nm thicknesses. A Maxtek RQCM instrument was used to measure the resonant frequency change when the IL coated Au QCM was exposed to various tested gases. In this study, the frequency change of all gases was mainly contributed by mass change.

Results and Discussion

Electrochemical system design and validation.— Most early literature reported the adsorption/dissolution of small gas molecules into IL double layer by introducing the analytes through the bulk of the ILs, and their results confirmed that adsorption/dissolution of small gas molecules in ILs significantly affect the IL EDL properties.[23,43,44] However, the results of adsorption/dissolution of small gas molecules on IL double layer properties were only qualitative discussed due to the multiple processes in both the IL double layer and bulk regions. Additionally, the thickness and the microscopic structure of IL EDL have not been well defined. For example, sum frequency generation spectroscopy studies showed that ions were organized in the Helmholtz layer at the interface,[45–48] but AFM studies[49–51] presented a well-defined structural organization of an IL at a Au(111) electrode interface with three structurally distinct regions: the interfacial (innermost) layer composed of ions in direct contact with the electrode; the transition region over which the pronounced interfacial layer structure decays to the bulk region. The innermost layer, which templates ion arrangements in the transition zone, is much more structured, and the ions form a single layer at the surface to screen the electrode charge.[23,31] For a systematic and quantitative evaluation of IL EDL properties, it is critical that the analyte is directly introduced to the innermost layer of IL–electrified metal interface rather than through the bulk of ILs. This technical consideration is important since it immediately minimizes the uncertainty due to analyte mass transport in the transition and bulk regions of the IL and greatly simplifies the response mechanisms.

For this reason, an innovative electrochemical cell was designed as shown in Figure 2a, and all three electrodes of the electrochemical cell were coated onto a porous membrane (Figure 2c). The single plane structure of the electrodes allows formation of a controlled thin IL film and maintains the good electrochemical contact within the electrodes. To demonstrate the suitability of the setup and identify the sensing mechanism, we tested the flow of the gas from both sides of the IL film (i.e. from the side of the interfacial region, pathway 2 in Figure 2b, as well as from the side of bulk region, pathway 1 in Figure 2b). Figure 3 shows the methane response through these two different pathways. Methane introduced directly to the IL/electrode interfacial region at 20th second gives a faster response time ((T_{90}) = 8 seconds) in comparison to methane that was introduced via the IL bulk (T_{90}) = 98 seconds). The mass transport of methane in the

Downloaded on 2016-09-15 to IP 134.197.85.26 address. Redistribution subject to ECS terms of use (see ecsdl.org/site/terms_use) unless CC License in place (see abstract).

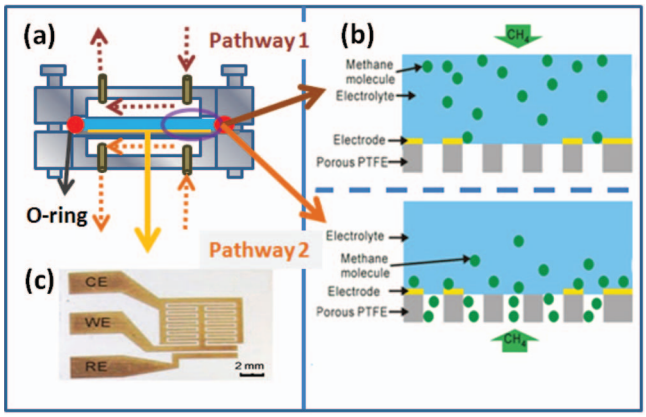


Figure 2. (a) Schematic diagram of side-view of electrochemical testing cell. (b) Schematic diagrams of methane mass transport processes via two mass transport pathways in this study. (c) Photo of the interdigited electrode used in this study.

IL transition and bulk regions contributes to the slow response due to the high viscosity of IL and the thickness-dependent mass transport processes. The maximum capacitances measured in both cases are identical. These results confirm that the slow reorientation of IL[33,52] in the bulk and transition regions does not change the IL-electrode interfacial structure, and that the capacitance change of the whole system primarily comes from the interface when exposed to the analyte methane. The results show that the double layer of the IL/electrode interface could be recognized as the response layer while the transition zone and bulk region of the IL-electrode interface contribute little to the overall differential capacitance change.

Effect of methane on the potential dependent differential capacitance at the IL–electrified electrode interface.— The EIS experiments can reveal the capacitive nature of the electrode/electrolyte interface. However, the capacitance measured reflects the overall capacitance response of outer Helmholtz plane and the diffuse region of the double layer at the IL-electrode interface. Since the total capacitance depends on the reciprocals of the two separate contributions, it is the smallest capacitance that dominates overall capacitance of the IL-electrode interface. The differential capacitance vs. potential curves at the $[C_4mpy][NTf_2]$ and mesoporous gold electrode interface were

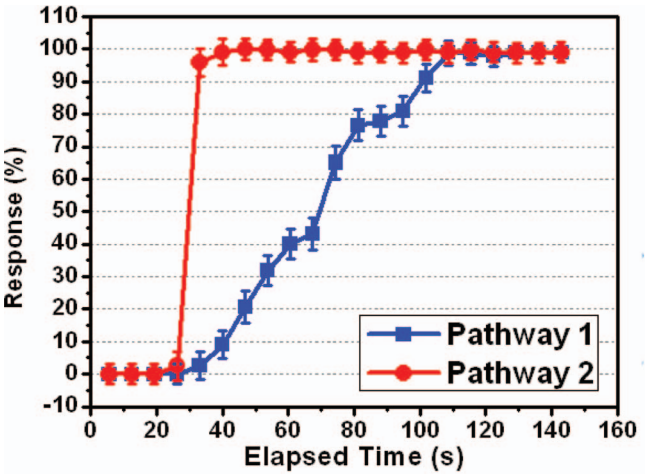


Figure 3. Normalized electrochemical impedance response obtained at 1 Hz at −0.3 V. 5% methane introduced at 20th second via two pathways shown in Figure 2a. In Pathway 1, methane flows from the side of bulk IL region, and in Pathway 2 methane flows from the side of interfacial region via the PTFE Teflon.

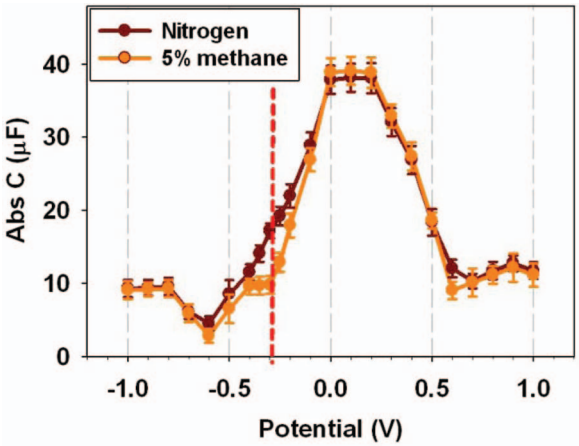


Figure 4. The capacitance-potential curves at the exposure of nitrogen or 5% methane at 1 Hz. Potential scanned from −0.8 V to 0.8 V. No faradaic processes in this potential window for the gases tested. Each potential was hold until capacitance values reach to a constant.

characterized under two conditions, one with 100% nitrogen and another with 5% methane exposure. The minimum or maximum values of capacitance have been reported around the potential of zero charge (PZC) in several commercial ILs.[53,26] Figure 4 shows the typical bell-shaped capacitance vs. potential curves for both conditions. The experimentally determined maximum capacitance at the PZC was shown to be three times of that in a typical aqueous solution.[26,54,55] In our study, the same PZCs (∼ 0.1 V) were found in the two conditions, suggesting that the introduction of the neutral molecules do not affect the overall charge on the IL interface. When the potential is more negative than −0.8 V or more positive than 1.0 V, the capacitance vs. potential curves at 5% methane and 100% nitrogen conditions were overlapped. It was rationalized that, at high positive or negative DC bias voltages, the strong correlation between anions and cations in the IL produces an ordering of several layers of the IL at the interface under the influence of the high electric field which, prevents the methane or nitrogen molecules from adsorbing on the electrode. The capacitance vs. potential curves show a significant decrease of capacitance at the bias potential of −0.3 V for the 5% methane condition compared to the pure nitrogen condition. As shown by others, when a voltage is applied across the electrode-electrolyte interface, the charge interactions cause counter ions to condense onto the electrode surface to form compact ion-image dipoles.[26] Since the surface density of dipoles is lowest at the PZC, the incorporation of an additional dipole due to analyte adsorption or dissolution in an IL will require minimum energy. Our findings suggest that the double layer property at −0.3 V DC bias potential is ideal for methane incorporation due to methane's specific size and polarity. The change of the double layer property likely involves a change of double layer thickness and order by adsorbing methane molecule to the interface, similar to those reported in a CO/platinum system.[23] The bias potential of −0.3 V was used throughout the remaining experimental work in this study.

Methane quantification with differential capacitance on the IL-electrode interface.— The Bode plots of the EIS impedance spectrum at the IL-Au electrode between 100 mHz and 10 kHz for exposure of different methane concentrations are shown in Figure 5a. In the low frequency range (100 mHz–10 Hz), the phase angle is close to −90° confirming the IL-Au electrode interface behaves like a pure capacitor. At −90° phase angle, the real part of complex capacitance defines the capacitance of system[41], which is contributed by the double layer of the IL-electrode interface. Figure 5b plots the real part of complex capacitance in the frequency range of 100 mHz to 10 kHz with different methane concentrations. At low frequencies, the IL-electrode interface capacitance was very sensitive toward methane. We selected a frequency of 1 Hz to plot the capacitance vs. methane

Downloaded on 2016-09-15 to IP 134.197.85.26 address. Redistribution subject to ECS terms of use (see ecsdl.org/site/terms_use) unless CC License in place (see abstract).

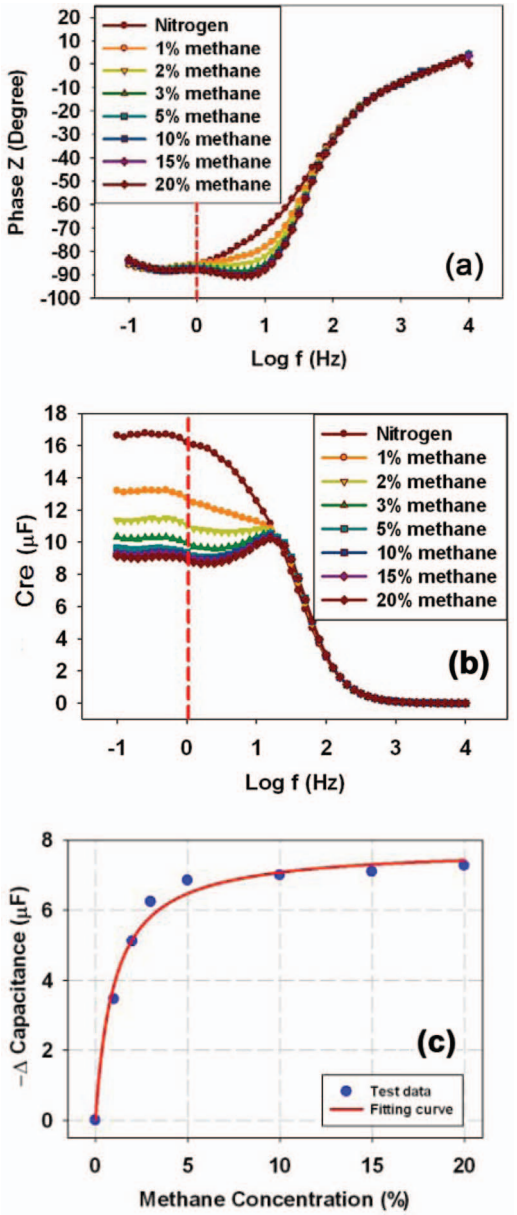


Figure 5 (a). Phase vs. frequency curves at different methane concentrations in the frequency range of 100 mHz to 10 kHz. (b) Plots of real part of complex capacitance at different methane concentrations. (c) Change of Cre at 1 Hz in Figure 5b vs. methane concentrations. [C4mpy][NTf2] is the IL and DC bias is −0.3 V.

concentration curve, shown in Figure 5c. The relationship of the capacitance vs. methane concentration is nonlinear, and the capacitance decreased from 16.2 μF to 8.8 μF in the presence of 20% methane. These measured capacitance values have the same order of magnitude as the double layer capacitance data reported by other groups.[23,33,56]

Physical origins of capacitance response of IL EDL and Langmuir adsorption model.— The IL-Au interfacial capacitance change upon methane exposure could be explained as follows. Under open circuit potential, a double layer with a well-defined ionic structure was formed at the IL-Au electrode interface by adsorption and cohesive interactions (Coulombic, van der Waals, hydrogen bonding, solvophobic forces) of anions and cations (Figure 1 and 6a). When a small negative DC bias potential close to PZC (−0.3 V) was applied at the gold working electrode, the cations of the IL were attracted to the gold surface of the working electrode, forming a Helmholtz layer

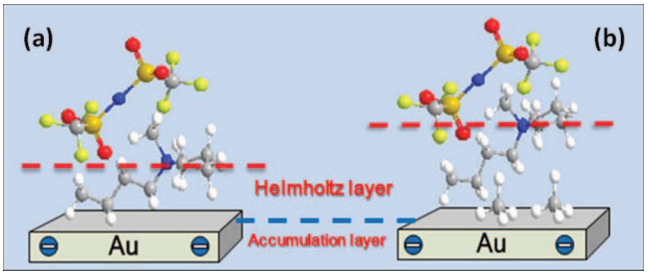


Figure 6. Illustration of innermost layer of the IL-Au interface at −0.3 V (i.e. the Helmholtz layer) (a) without methane; (b) with methane.

with a thickness (d) in nanometer range (Figure 6a). Because the IL EDL is smaller than 1 nm, as confirmed by AFM,[51] which is close to the size of gas molecules, the IL EDL is perturbed easily by exposure to the gas analyte. The gas present on the electrode surface could result in the reconstruction of the electric double layer, as has been observed in aqueous solutions as well.[57,58] Here, methane is electrochemically inert at −0.3 V, so no faradaic process of methane occurs at −0.3 V. Methane is a non-polar molecule, so there is no electrostatic resistance for methane to be incorporated into the EDL. Therefore, methane molecules could have permeated to the IL-electrode interface quickly and subsequently changed the double layer structure and increased the EDL's thickness, as shown in Figure 6b. The solubility of methane in [C_4mpy][NTf_2] is very low. Compared with other gases, methane has strong adsorption on a metal electrode via the C-H-metal bond.[59–62] Thus, adsorption should be predominant and thus methane would accumulate in the innermost layer rather than being dissolved into the transition and bulk IL layers. We can assume a Langmuir adsorption model for this process, quantitatively described by[63]

$$CH_4 + IL/Au \leftrightarrow CH_4 - IL/Au(ads) \quad [1]$$

$$\theta = \frac{K_1 C_{CH_4,IL}}{1 + K_1 C_{CH_4,IL}} \quad [2]$$

where θ is the surface coverage of adsorbate on the working electrode, $C_{CH4,IL}$ is the concentration of CH_4 in IL, K_1 is the ratio of the forward and reverse rate constants at the CH_4 adsorption equilibrium. Since $C_{CH4,IL}$ is proportional to the CH_4 concentration (C_{CH4}) in the gas phase with Henry law, k_H is defined as the Henry constant:

$$k_H = \frac{C_{CH_4,IL}}{C_{CH_4}} \quad [3]$$

Equation 2 can thus be rewritten as

$$\theta = \frac{K_1 K_H C_{CH_4}}{1 + K_1 K_H C_{CH_4}} \quad [4]$$

Defining C_{dl0} as double-layer capacitance value when surface coverage θ is zero and C_{dl1} as double-layer capacitance value when surface coverage θ is one. The double-layer capacitance C_{dl} can be expressed in terms of θ as

$$C_{dl} = C_{dl0} \cdot (1 - \theta) + C_{dl1} \cdot \theta \quad [5]$$

Combining equation 2 and 5, we obtain equation 6:

$$C_{dl} = C_{dl0} + (C_{dl1} - C_{dl0}) \cdot \frac{K_1 K_H C_{CH_4}}{1 + K_1 K_H C_{CH_4}} \quad [6]$$

From equation 6, the capacitor change $\Delta C_{dl} = C_{dl} - C_{dl0}$ in Figure 5c can be presented as

$$\Delta C_{dl} = (C_{dl1} - C_{dl0}) \cdot \frac{K_1 K_H C_{CH_4}}{1 + K_1 K_H C_{CH_4}} \quad [7]$$

Equation 7 reveals the relationship between the change of the double-layer capacitance and CH_4 concentration. Using this expression, the data from Figure 5b at 1 Hz can be plotted to show the C_{dl}

Downloaded on 2016-09-15 to IP 134.197.85.26 address. Redistribution subject to ECS terms of use (see ecsdl.org/site/terms_use) unless CC License in place (see abstract).

response as a function of C_{CH4}, as shown in Figure 5c. Using equation 7 to model the experimental data, the fitting curve is plotted as a red line in Figure 5c. The excellent fit between the experimental results with the Langmuir model ($R^2 = 0.996$), further supports our proposed response mechanisms of the IL-Au double layer sensing.

$$\Delta C_{dl} = 7.4\mu F \cdot \frac{101C_{CH_4}}{1 + 101C_{CH_4}} \quad [8]$$

From Figure 5, we obtained that $C_{dl0} = 16.2\ \mu F$ and $C_{dl1} = 8.8\ \mu F$ at zero and 100% methane coverage, respectively. The relationship between C_{dl} and C_{CH4} can be expressed as :

$$C_{dl} = 16.2\mu F - 7.4\mu F \cdot \frac{101C_{CH_4}}{1 + 101C_{CH_4}} \quad [9]$$

Using the capacitance value at zero (C_{dl0}) and 100% coverage (C_{dl1}), if we use 11.7 F/m as the relative static permittivity of $[C_4mpy][NTf_2]$,[63] the thicknesses of the double layer for zero methane coverage can be calculated to be about 0.66 nm which is consistent with the magnitude of the IL adsorption layer thickness measured by STM.[49] The thickness of the EDL with 100% methane coverage is about 1.72 nm, which is a little larger than the sum of the thickness of the IL and the methane molecule diameter (Supporting material Table S1). Assuming the IL's permittivity is not affected by methane, the thickness of the EDL is increased by 160%. It can be explained by the assumption that the adsorption of methane into the IL EDL affects the distribution of electric field and reduces the EDL capacitance. Our results show that the IL EDL is highly sensitive to methane. The sensitivity is especially high at low concentration, which is consistent with the Langmuir adsorption model. In the range of interests for methane detection (1–5%), the sensitivity is −3.46 μF/% at 1% of CH_4 concentration and −0.31 μF/% at 5% of CH_4 concentration. Such high sensitivity in the low concentration range of methane is very suitable for methane detection in many real world applications.

Interference and selectivity of the IL-electrode interface for methane detection.— We measured the interfering responses of common atmospheric gases (i.e. N_2, CO_2, O_2, NO_2, NO, SO_2, H_2O and an volatile organic compound cyclohexane) under the selected DC bias potential (−0.3 V) at the IL-electrode interface. The response in the presence of pure nitrogen was used as the blank. Figure 7a summarizes the relative signal of each gas with respect to nitrogen. Figure 7b summarizes the maximum interference to 5% methane in nitrogen. The concentrations of all the tested gases are selected based either on their typical concentrations or their maximum permissible concentrations in the atmosphere. Details are described in the support information. Methane gives the highest signal among all other gases. NO, NO_2 and water are showing higher interfering signals than that of CO_2, O_2, H_2 and cyclohexane.

The response mechanisms of interferences from these tested gases are complex which could depend on the combination of several factors including the size of the interfering molecules, the solubility of the interfering molecules in the IL, and the adsorption of the interfering molecules at the IL-Au interface. According to the literature[23], the IL-electrode interface double layer thickness of $[C_4mpy][NTf_2]$-Au is around 0.5∼1.2 nm which matches the molecular diameter of methane (about 0.38 nm). Hydrogen and cyclohexane are non-polar molecules. There is almost no response to these two gases under same experimental conditions at the IL-Au interface. It is explained that the size of hydrogen with molecular size of 0.289 nm is too small to generate effective change of the double layer capacitance and the size of cyclohexane with molecular diameter about 0.60 nm is too larger and was overscreened by the ion pairs of the IL from the electrode surface.

Beside the molecule size, solubility of interfering gases in the IL and the adsorption of the interfering gases at the IL-Au interface could contribute to the gas selectivity. Interactions between the anion of IL and polar molecules can increase the solubility of gases in the ILs.[65–67] QCM can effectively quantify the adsorption and partition of gases in

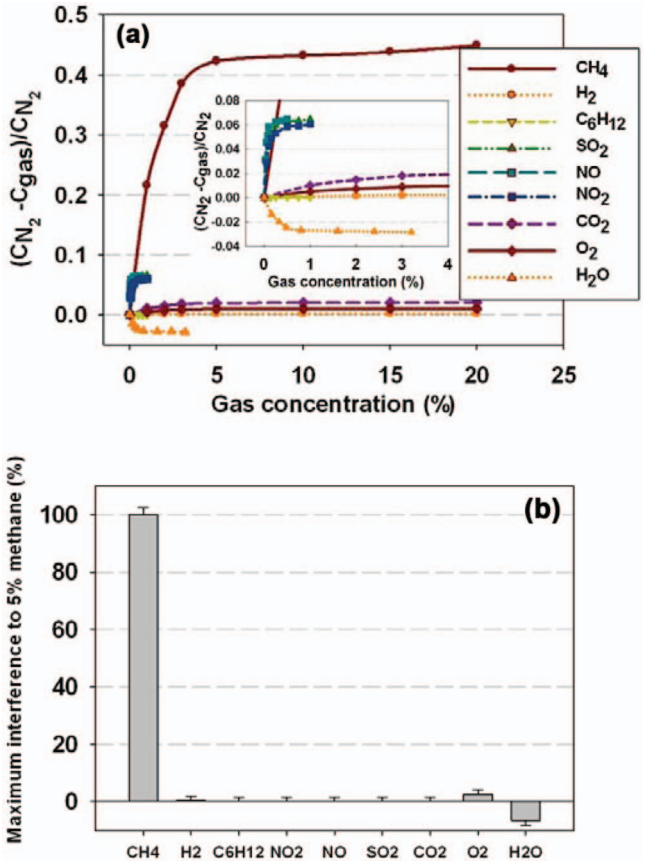


Figure 7. (a) The relative sensitivity of common gases in the air to methane. The inset graph is at low gas concentrations. Capacitances were recorded at DC bias potential −0.3 V and AC frequency at 1 Hz. (b) The relative interference which is the ratio of the capacitance signals measured at the conditions when the interfering gases are at maximum permissible concentrations in air and methane concentration at 5% (v/v) respectively. Details are shown in supporting information.

an IL thin film[68] and was used in this work to compare the adsorption and dissolution properties of various gases in the $[C_4mpy][NTf_2]$. As shown in Figure S3, NO_2, NO, CO_2, SO_2 have much higher solubility in $[C_4mpy][NTf_2]$ than that of oxygen and methane. At −0.3 V, there is no redox activity of NO_2, NO and SO_2.[16,69–71] Although the IL double layer thickness is larger than the molecular size of these gases, which means all of these gases could adsorb at the IL double layer. Our results imply that these gases will dissolve more easily into the bulk. The negative DC bias potential also reduced their adsorption at the IL-gold electrode via Au-N and Au-S coordinate bonds. This rationalization is consistent with other groups' reports.[11,66,71–73] Furthermore, the maximum permissible concentrations of these gases in the atmosphere are all lower than 50 ppm. The interferences from these gases are negligible at such real world concentration ranges. Non-polar molecules such as O_2 and CO_2 have much less adsorption at IL-Au interface. O_2 and CO_2 likely dissolve into bulk of IL which gives little influence on EDL of the electrified IL-electrode interface.[74–77]

As shown in Figure 7a and 7b, in comparison with methane and all other tested gases, for which high concentration of gases decreases the IL-Au capacitance, the presence of water was found to increase the capacitance of the IL-Au double layer, thus indicating a negative signal correlation in the presence of water. Small amounts of water could adsorb at the IL-electrode interface because the Au electrode surface is hydrophilic. Since the 100% relative humidity is only about 3.1 vol.% of water in air, this amount of water will not significantly change the bulk viscosity or conductivity of a hydrophobic IL. Thus,

Downloaded on 2016-09-15 to IP 134.197.85.26 address. Redistribution subject to ECS terms of use (see ecsdl.org/site/terms_use) unless CC License in place (see abstract).

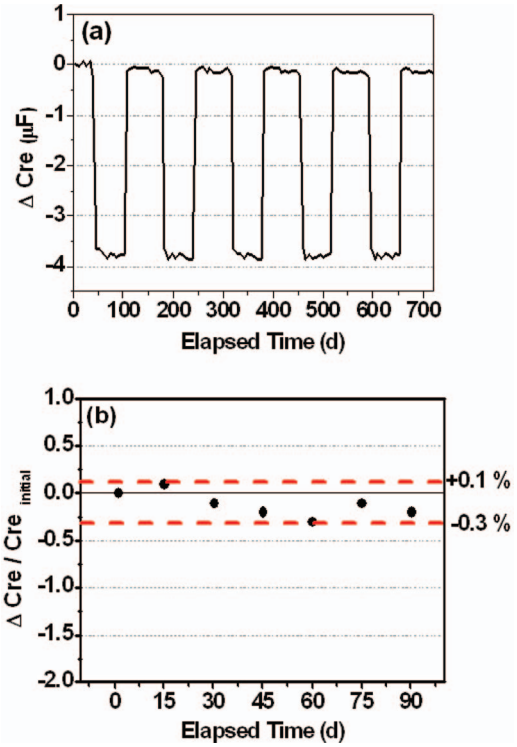


Figure 8. (a) C_{re} measured over five cycles of alternate exposure to 5% methane with nitrogen as the carrier gas. The nitrogen gas flow remained constant at 200 sccm. Applied DC potential is −0.3 V vs. Au quasi reference electrode. AC frequency is at 1 Hz. (b) methane sensor stability over 90 days (signal obtained at 5% methane response) Δcapacitance = Cre – $Cre_{(first\ day)}$.

it is most likely that water would permeate into the IL-Au interface, and a new double layer with water molecules highly coordinated with ILs would form owing to water's high polarity thus changing the IL-Au interface organization. The electric field at the IL-Au interface facilitates the interactions of water with IL molecules. Compared to the IL-Au interface in the absence of water, the capacitance of the IL-Au double layer formed in the presence of water has been reported to be larger due to the higher permittivity of water (81 F/m) than that of $[C_4mpy][NTf_2]$ (11.7 F/m).[64] In our current interests of exploring the EDL of the IL-electrode interface as a capacitance sensor, it is beneficial to use highly viscous and hydrophobic ILs to minimize the adsorption and dissolution of H_2O molecule to the IL-electrode interface. Figure 7a shows that all responses follow the trends of Langmuir adsorption isotherm, which not only supports the response mechanism proposed earlier but also allows for the calibration of analyte response in the presence of interfering species. The mechanism of gas selectivity is complicated due to multiple parameters influencing the gas selectivity and is under further investigation.

Reversibility and Stability of the IL-electrode interface sensory system.— In order to study the reversibility and stability of our IL sensor system, two experiments were performed at the presence of methane. Figure 8a plots the C_{dl} (1 Hz) vs. time curve when the sensor was repeatedly exposed to 5% methane in nitrogen for five cycles. The result shows a complete reversibility. The response to methane is quite rapid with a response time of ∼8 seconds. This reflects the time necessary for exchange of the pure nitrogen carrier gas with 5% methane-containing nitrogen in the cell coupled with the equilibration between the methane and the IL electrolyte. Compared with other electrochemical sensing methods, EIS is a noninvasive technique and there is no redox reaction under −0.3 V. As shown in Figure 8b, the capacitance at 1 Hz with 5% methane was measured over a period of 90 days at the same experimental condition as Figure 8a. The signals are normalized to the first day's signal. The values were calculated by taking the mean of at least three measurements. Figure 8b demonstrates the response stability to 5% methane over 90 days, during which a capacitance change of ± 0.3% was observed, revealing influence of methane to IL EDL was stable and reproducible.

Conclusions

This study shows that the nature of the ion arrangements at an IL-electrified interface provides the needed chemical sensitivity and selectivity for gas sensing based on the capacitance of IL–electrified metal interface. By selection of the IL $[C_4mpy][NTf_2]$ with an EDL structure matches to the properties of the methane and by selecting the DC bias voltage at −0.3 V based on the capacitance-potential curve maxima, highly sensitive and selective methane sensor was demonstrated with rapid and reversible response. Our results show that the methane response signal fits the Langmuir adsorption model and can be quantified with Langmuir adsorption isotherms. The gas selectivity for methane is validated in the presence of SO_2, CO_2, NO_2, NO, O_2, H_2O and cyclohexane. The selectivity comes from the unique highly ordered arrangement of ions in the innermost layer of IL-electrode interface that is potential dependent. The degree of ordered structure at IL-electrode interface can be tuned by the applied bias potential on the electrode and by the unique molecular structure of the IL ions. The high viscosity of ILs, which is usually considered a limitation to practical electrochemical applications due to slow rate of mass transport, is an advantage in capacitance measurement[78] due to the more ordered and concentrated double layer. This innovative approach overcomes the hysteresis effect and the slow rearrangement of bulk ILs caused by the potential change. Currently, we are performing research to account for more factors in selectivity and extend this strategy to create gas sensors for other analytes. This work provides both fundamental and applied knowledge related to IL-electrode double layer that could impact many important applications including sensors, batteries and electrocatalysis, material chemistry and electronics.

Electronic Supplementary Information (ESI) Available

Figure S1-S3 and Table S1 are provided as supplementary information.

Acknowledgment

Support from NIOSH grants (R21 and R01) are greatly acknowledged. We thank Dr. Mike Sevilla for helpful discussions and Abdul Rehman for contributions to proofread and editing.

References

1. M. Armand, F. Endres, D. R. MacFarlane, H. Ohno, and B. Scrosati, *Nat. Mater.*, **8**(8), 621 (2009).
2. P. Simon and Y. Gogotsi, *Nat. Mater.*, **7**(11), 845 (2008).
3. T. P. Lodge, *Science*, **321**(5885), 50 (2008).
4. M. Y. Lui, L. Crowhurst, J. P. Hallett, P. A. Hunt, H. Niedermeyer, and T. Welton, *Chem. Sci.*, **2**(8), 1491 (2011).
5. Y. Meng, L. Aldous, and R. G. Compton, *The Journal of Physical Chemistry C*, **115**(29), 14334 (2011).
6. C. A. Angell, N. Byrne, and J. P. Belieres, *Accounts Chem. Res.*, **40**(11), 1228 (2007).
7. R. J. Chen, H. Q. Zhang, and F. Wu, *Prog. Chem.*, **23**(2–3), 366 (2011).
8. E. S. Forzani, D. L. Lu, M. J. Leright, A. D. Aguilar, F. Tsow, R. A. Iglesias, Q. Zhang, J. Lu, J. H. Li, and N. J. Tao, *J. Am. Chem. Soc.*, **131**(4), 1390 (2009).
9. F. Chen, Q. Qing, J. L. Xia, J. H. Li, and N. J. Tao, *J. Am. Chem. Soc.*, **131**(29), 9908 (2009).
10. L. Chen, D. Huang, Y. Zhang, T. Dong, C. Zhou, S. Ren, Y. Chi, and G. Chen, *Analyst*, **137**(15), 3514 (2012).
11. D. R. MacFarlane, S. A. Forsyth, J. Golding, and G. B. Deacon, *Green Chem.*, **4**(5), 444 (2002).
12. L. H. J. Xiong, A. M. Fletcher, S. G. Davies, S. E. Norman, C. Hardacre, and R. G. Compton, *Chem. Commun.*, **48**(46), 5784 (2012).
13. R. Toniolo, N. Dossi, A. Pizzariello, A. P. Doherty, and G. Bontempelli, *Electroanal*, **24**(4), 865 (2012).

Downloaded on 2016-09-15 to IP 134.197.85.26 address. Redistribution subject to ECS terms of use (see ecsdl.org/site/terms_use) unless CC License in place (see abstract).

14. Z. Wang, P. Lin, G. A. Baker, J. Stetter, and X. Zeng, *Anal. Chem.*, **83**(18), 7066 (2011).
15. K. Cui, D. D. Zhu, W. Cui, X. M. Lu, and Q. H. Lu, *J. Phys. Chem. C*, **116**(10), 6077 (2012).
16. M. C. Buzzeo, C. Hardacre, and R. G. Compton, *Anal. Chem.*, **76**(15), 4583 (2004).
17. S. Y. Yang, F. Cicoira, R. Byrne, F. Benito-Lopez, D. Diamond, R. M. Owens, and G. G. Malliaras, *Chem. Commun.*, **46**(42), 7972 (2010).
18. P. Werle, R. Mücke, and F. Slemr, *Applied Physics B Photophysics and Laser Chemistry*, **57**(2), 131 (1993).
19. J. R. Stetter and J. Li, *Chem. Rev.*, **108**(2), 352 (2008).
20. A. Tuantranont, A. Wisitsora-at, P. Sritongkham, and K. Jaruwongrungsee, *Anal. Chim. Acta*, **687**(2), 114 (2011).
21. J. M. Rheaume and A. P. Pisano, *Ionics*, **17**(2), 99 (2011).
22. H. T. Yuan, H. Shimotani, A. Tsukazaki, A. Ohtomo, M. Kawasaki, and Y. Iwasa, *J. Am. Chem. Soc.*, **132**(19), 6672 (2010).
23. S. Baldelli, *Accounts Chem. Res.*, **41**(3), 421 (2008).
24. J. Chmiola, G. Yushin, Y. Gogotsi, C. Portet, P. Simon, and P. L. Taberna, *Science*, **313**(5794), 1760 (2006).
25. M. Z. Bazant, B. D. Storey, and A. A. Kornyshev, *Phys. Rev. Lett.*, **106**(4), 046102 (2011).
26. M. S. Loth, B. Skinner, and B. I. Shklovskii, *Phys. Rev. E*, **82**(5), 056102-1 (2010).
27. V. Lockett, M. Horne, R. Sedev, T. Rodopoulos, and J. Ralston, *Phys. Chem. Chem. Phys.*, **12**(39), 12499 (2010).
28. P. S. Santos, R. A. Ando, L. J. A. Siqueira, F. C. Bazito, and R. M. Torresi, *J. Phys. Chem. B*, **111**(30), 8717 (2007).
29. L. M. G. Sanchez, G. W. Meindersma, and A. B. de Haan, *Chem. Eng. Res. Des.*, **85**(A1), 31 (2007).
30. G. A. Feng, R. Qiao, J. S. Huang, S. Dai, B. G. Sumpter, and V. Meunier, *Phys. Chem. Chem. Phys.*, **13**(3), 1152 (2011).
31. R. Hayes, N. Borisenko, M. K. Tam, P. C. Howlett, F. Endres, and R. Atkin, *J. Phys. Chem. C*, **115**(14), 6855 (2011).
32. R. Hayes, S. Z. El Abedin, and R. Atkin, *J. Phys. Chem.*, **113**(20), 7049 (2009).
33. M. Druschler, B. Huber, S. Passerini, and B. Roling, *J. Phys. Chem. C*, **114**(8), 3614 (2010).
34. V. W. H. Lau, L. G. A. van de Water, A. F. Masters, and T. Maschmeyer, *Chem-Eur. J.*, **18**(10), 2923 (2012).
35. M. S. Kilic, M. Z. Bazant, and A. Ajdari, *Phys. Rev. E*, **75**(2), (2007).
36. H. Jin, G. A. Baker, S. Arzhantsev, J. Dong, and M. Maroncelli, *The Journal of Physical Chemistry B*, **111**(25), 7291 (2007).
37. T. Ohsaka, M. T. Alam, M. M. Islam, and T. Okajima, *J. Phys. Chem. C*, **112**(42), 16600 (2008).
38. P. Kilaru, G. A. Baker, and P. Scovazzo, *Journal of Chemical & Engineering Data*, **52**(6), 2306 (2007).
39. A. K. Burrell, R. E. D. Sesto, S. N. Baker, T. M. McCleskey, and G. A. Baker, *Green Chemistry*, **9**(5), 449 (2007).
40. S. N. Baker, T. M. McCleskey, S. Pandey, and G. A. Baker, *Chemical Communications*, (8), 940 (2004).
41. M. E. Orazem and B. Tribollet, *Electrochemical Impedance Spectroscopy*, Wiley InterScience, New York (2008).
42. X. Jin, L. Yu, D. Garcia, R. X. Ren, and X. Zeng, *Anal. Chem.*, **78**(19), 6980 (2006).
43. C. Aliaga and S. Baldelli, *J. Phys. Chem. C*, **112**(8), 3064 (2008).
44. S. Baldelli and I. S. Martinez, *J. Phys. Chem. C*, **114**(26), 11564 (2010).
45. S. Baldelli, *J. Phys. Chem. B*, **107**(25), 6148 (2003).
46. S. Baldelli, *J. Phys. Chem. B*, **109**(27), 13049 (2005).
47. S. Baldelli, *Abstr. Pap. Am. Chem. S*, **231** (2006).
48. S. Baldelli, J. M. Bao, W. Wu, and S. S. Pei, *Chem. Phys. Lett.*, **516**(4–6), 171 (2011).
49. R. Atkin, S. Z. El Abedin, R. Hayes, L. H. S. Gasparotto, N. Borisenko, and F. Endres, *J. Phys. Chem. C*, **113**(30), 13266 (2009).
50. F. Endres, R. Atkin, N. Borisenko, M. Druschler, S. Z. El Abedin, R. Hayes, B. Huber, and B. Roling, *Phys. Chem. Chem. Phys.*, **13**(15), 6849 (2011).
51. F. Endres, N. Borisenko, S. Z. El Abedin, R. Hayes, and R. Atkin, *Faraday Discuss*, **154**, 221 (2012).
52. R. G. Compton, L. E. Barrosse-Antle, L. Aldous, C. Hardacre, and A. M. Bond, *J. Phys. Chem. C*, **113**(18), 7750 (2009).
53. C. Nanjundiah, S. F. McDevitt, and V. R. Koch, *J. Electrochem. Soc.*, **144**(10), 3392 (1997).
54. M. T. Alam, M. M. Islam, T. Okajima, and T. Ohsaka, *J. Phys. Chem. C*, **111**(49), 18326 (2007).
55. H. L. F. Von Helmholtz, *P Ieee*, **92**(5), 868 (2004).
56. E. Lust, L. Siinor, and K. Lust, *Electrochem. Commun.*, **12**(8), 1058 (2010).
57. D. M. Kolb, *Angew. Chem. Int. Edit*, **40**(7), 1162 (2001).
58. J. Schneider, C. Franke, and D. M. Kolb, *Surf. Sci.*, **198**(1–2), 277 (1988).
59. A. Bukoski, H. L. Abbott, and I. Harrison, *J. Chem. Phys.*, **123**(9), 094707 (2005).
60. A. Bukoski, D. Blumling, and I. Harrison, *J. Chem. Phys.*, **118**(2), 843 (2003).
61. G. R. Schoofs, C. R. Arumainayagam, M. C. Mcmaster, and R. J. Madix, *Surf. Sci.*, **215**(1–2), 1 (1989).
62. N. M. Galea, D. Knapp, and T. Ziegler, *J Catal*, **247**(1), 20 (2007).
63. L. Yu, X. X. Jin, and X. Q. Zeng, *Langmuir*, **24**(20), 11631 (2008).
64. H. Weingartner, P. Sasisanker, C. Daguenet, P. J. Dyson, I. Krossing, J. M. Slattery, and T. Schubert, *J. Phys. Chem. B*, **111**(18), 4775 (2007).
65. F. Llovell, R. M. Marcos, N. MacDowell, and L. F. Vega, *J. Phys. Chem. B*, **116**(26), 7709 (2012).
66. G. K. Cui, C. M. Wang, J. J. Zheng, Y. Guo, X. Y. Luo, and H. R. Li, *Chem. Commun.*, **48**(20), 2633 (2012).
67. C. Wang, J. Zheng, G. Cui, X. Luo, Y. Guo, and H. Li, *Chem. Commun.*, (2013).
68. X. X. Jin, L. Yu, D. Garcia, R. X. Ren, and X. Q. Zeng, *Anal. Chem.*, **78**(19), 6980 (2006).
69. L. E. Barrosse-Antle, D. S. Silvester, L. Aldous, C. Hardacre, and R. G. Compton, *J. Phys. Chem. C*, **112**(9), 3398 (2008).
70. L. E. Barrosse-Antlle, C. Hardacre, and R. G. Compton, *J. Phys. Chem. B*, **113**(4), 1007 (2009).
71. T. L. Broder, D. S. Silvester, L. Aldous, C. Hardacre, and R. G. Compton, *J. Phys. Chem. B*, **111**(27), 7778 (2007).
72. C. M. Wang, G. K. Cui, X. Y. Luo, Y. J. Xu, H. R. Li, and S. Dai, *J. Am. Chem. Soc.*, **133**(31), 11916 (2011).
73. J. Huang, A. Riisager, P. Wasserscheid, and R. Fehrmann, *Chem. Commun.*, (38), 4027 (2006).
74. M. E. Perez-Blanco and E. J. Maginn, *J. Phys. Chem. B*, **114**(36), 11827 (2010).
75. X. H. Li, G. C. Schatz, and D. J. Nesbitt, *J. Phys. Chem. B*, **116**(11), 3587 (2012).
76. C. Wu, T. P. Senftle, and W. F. Schneider, *Phys. Chem. Chem. Phys.*, **14**(38), 13163 (2012).
77. X. P. Zhang, X. C. Zhang, H. F. Dong, Z. J. Zhao, S. J. Zhang, and Y. Huang, *Energ. Environ. Sci.*, **5**(5), 6668 (2012).
78. T. Ohsaka, M. T. Alam, M. M. Islam, and T. Okajima, *Electrochem. Commun.*, **9**(9), 2370 (2007).

Downloaded on 2016-09-15 to IP 134.197.85.26 address. Redistribution subject to ECS terms of use (see ecsdl.org/site/terms_use) unless CC License in place (see abstract).